

Effect of orientations on cyclic deformation behavior of Ag and Cu single crystals: Cyclic stress–strain curve and slip morphology

P. Li, Z.F. Zhang^{*}, S.X. Li, Z.G. Wang

*Shenyang National Laboratory for Materials Science, Institute of Metal Research, Chinese Academy of Sciences,
72 Wenhua Road, 110016 Shenyang, China*

Received 29 November 2007; received in revised form 4 January 2008; accepted 6 January 2008
Available online 4 March 2008

Abstract

This work investigates the differences in the cyclic stress–strain (CSS) curves and surface slip morphologies of the fatigued Ag and Cu single crystals with different orientations. It is found that the average saturation resolved shear stress τ_s of Ag single crystal is ~ 6 MPa less than that of Cu single crystal with the same orientation. In addition, for the same kind of crystal, whether Cu or Ag, it seems that the saturation shear stress of coplanar double-slip-oriented single crystal is slightly higher than that of single-slip-oriented single crystal. In addition, the surface deformation morphologies (deformation bands and slip bands) are strongly dependent on the crystallographic orientations. As the crystallographic orientations of the crystals deviate from the best observation orientation $[1\bar{2}1]$ zone, on the one hand, the resolved shear stress τ_s rises and some braided slip bands (SB) appear on the crystal surface, and, on the other hand, the interacting angle between the primary slip bands and the deformation band II (DBII) changes from perpendicular to a gradually smaller angle. Based on the experimental results, the relationships between crystallographic orientation, CSS curves and slip morphologies (including DBII and SB) in the fatigued Ag and Cu single crystals are discussed.

© 2008 Acta Materialia Inc. Published by Elsevier Ltd. All rights reserved.

Keywords: Cyclic stress–strain curve; Single crystals; Slip morphology; Crystallographic orientation; Deformation band

1. Introduction

From the beginning of the 1950s, it has been generally recognized that without a systematic study of the entire process and nature of the fatigue damage mechanism in detail, there will be no fundamental understanding of the basic process of fatigue from the micro-scale level. Based on this understanding, in the past 40 years, especially in the 1970s and 1980s, many researches have contributed to progress in fatigue damage mechanisms. The most conclusive results were obtained from high-purity materials, especially from face-centered cubic (fcc) Cu single crystal [1–11]. The main results have been well reviewed by Basinski and Basinski [12]. The interesting points focused upon the establishment of cyclic stress–strain (CSS) curves, the

observations of persistent slip bands (PSB) and their corresponding dislocation structures, as well as fatigue crack initiation. In addition to the features above, the formation of deformation bands (DB) seems to be another important feature induced by cyclic deformation [13,14].

In Cu single crystal, it is well known that PSB with ladder-like structures often exist during cyclic deformation, and the related mechanisms have been widely investigated [12]. First, a two-phase (PSB and veins) model was proposed to explain the plastic strain localization in fatigued crystals [3,4]. After that, Mughrabi [5] proposed the famous CSS curve of Cu single crystal with single-slip orientation. The most important and interesting finding in the CSS curve is that a plateau region exists corresponding to the appearance of PSB. In order to reveal the evolution of PSB further, based on the diamond model of the Taylor–Nabarro matrix, Neumann [15,16] explored the decomposition of the vein structure and the formation of the wall

^{*} Corresponding author. Tel.: +86 2423971043.
E-mail address: zhfzhang@imr.ac.cn (Z.F. Zhang).

structure. It can be regarded as a significant attempt to discover the formation mechanism of PSB.

In actual polycrystalline materials, however, the orientation of grains is randomly distributed. Therefore, in order to broaden the research field further, it is necessary to study the influence of the crystallographic orientations on cycle deformation behavior. In this regard, Chen and Laird [8] measured the saturation resolved shear stress τ_s of various Cu single crystals within the standard stereographic triangle (including some with orientation near the three edges of the stereographic triangle). They found that the saturation resolved shear stress τ_s of all the crystals was ~ 28 MPa. They claimed that the saturation resolved shear stress τ_s and the plateau region in the CSS curve did not depend on the crystallographic orientations. Recently, Li et al. [17–21] systematically summarized the cyclic deformation behavior of Cu single crystals, especially for crystals with typical double- and multiple-slip orientations on three edges of the standard stereographic triangle. They thought that the orientations strongly influenced the CSS behavior of the above crystals, and the appearance or disappearance of a plateau in their CSS curves and the related saturation stress were inseparably associated with the active slip systems operating in the crystals and the mode and intensity of dislocation interactions among these slip systems.

With regard to DB, Mughrabi [5] found that the DB analogous to the kink band often occurred in single-slip-oriented Cu single crystals cyclically deformed at higher strain amplitude of $\sim 10^{-2}$. He believed that the relaxation of long-range internal stress might be responsible for the formation of DB. In addition, Li et al. [13] systematically investigated the formation and the interactions of various DB in fatigued Cu single crystals with different orientations. They found that the habit planes of DBI and DBII were close to (111) and $(\bar{1}01)$, respectively, and that they were perpendicular to each other.

In summary, cyclic deformation behavior in fcc crystals is composed of a CSS curve, surface slip morphology and dislocation patterns, which are all extremely sensitive to the crystal orientation. Compared with dislocation patterns, the CSS curve and slip morphology of single crystals display only their macroscopic characteristics. In addition to Cu crystals, there are also some investigations on the fatigue behavior of other fcc metals or alloys, e.g., Ni, Al and Cu–Al alloy single crystals [22–24]. It seems that the cyclic deformation behavior and saturation dislocation structure of Ni single crystals are closer to those of Cu single crystals. However, the cyclic deformation and dislocation structures of Al and Cu–Al single crystals displayed features significantly different from those of Cu and Ni single crystals. This indicates that different fcc crystals should behave with quite different fatigue properties and damage mechanisms. It is well known that Ag is one of the important fcc metals, but there are hardly any reports on its fatigue behavior, except for preliminary research available three decades ago [25]. The current research will systemat-

ically investigate the influence of the orientation on the CSS response, surface slip morphology (including DBII and SB) of Ag crystals in comparison with those of Cu single crystals. Finally, the reasons for the formation of different surface slip morphologies between Ag and Cu crystals are discussed.

2. Experimental procedures

To investigate the similarities and differences in the cyclic deformation behavior of various fcc crystals, Ag single crystal was prepared together with Cu single crystals with two different orientations. First, bulk Ag and Cu single crystals were grown separately from electrolytic silver of 99.999% purity and OFHC copper of 99.999% purity by the Bridgman method in a horizontal furnace. Secondly, fatigue specimens with two dimensions were cut by an electrospark cutting machine. The geometry and dimensions of the specimens for fatigue tests are illustrated in Fig. 1.

The crystal orientations of these specimens were determined by the electron back-scattering diffraction (EBSD) technique in a Cambridge S360 scanning electron microscope. Here, the stress axis orientation of Ag single crystal can be referred to as $[\bar{2}33]$. The stress axis orientations of the two Cu single crystals were determined to be $[\bar{2}36]$ and $[\bar{1}39]$, respectively. With the previous results on $[\bar{2}33]$ Cu single crystal and $[\bar{1}28]$ Ag single crystal, all the orientations of the Cu and Ag single crystals are illustrated in the stereographic triangle in Fig. 2. Before cyclic deformation, all the fatigue specimens were electro-polished carefully for surface observation. Symmetrical push–pull tests were performed on a Shimadzu servohydraulic testing machine under constant plastic strain control at room temperature in air. A triangle wave with a frequency range 0.1–1 Hz was used. All specimens were deformed cyclically up to the occurrence of saturation.

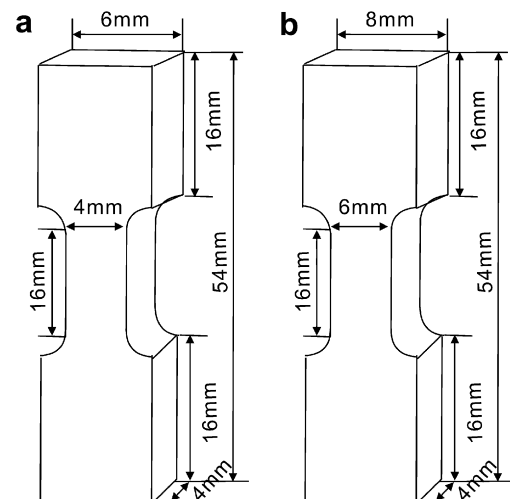


Fig. 1. Illustration of fatigue specimens: (a) $[\bar{1}39]$ Cu single crystal; (b) $[\bar{2}33]$ Ag single crystal; $[\bar{2}36]$ Cu single crystal.

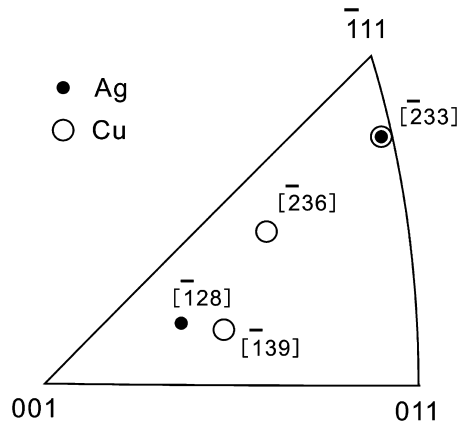


Fig. 2. Stereographic triangle showing the orientations of loading axis for Cu and Ag single crystals involved in this paper, where full circles represent Ag single crystal and open circles represent Cu single crystal.

After the fatigue tests, the surface slip morphologies of Cu and Ag single crystals were carefully observed by scanning electron microscope (SEM) on a LEO Super 35 instrument.

3. Results and discussion

For a better comparison, fatigue testing conditions and data on cyclic saturation in various Cu and Ag single crystals are summarized in Table 1, where γ_{pl} and τ_s are the plastic shear strain amplitude and saturation resolved shear stress, respectively. The sample number corresponds to the plastic shear strain amplitude and the corresponding cycles.

Table 1
Fatigue testing conditions and data for various copper and silver crystals

Orientation	Specimen no.	γ_{pl}	Cyclic no.	τ_s (MPa)	Investigators
[233]Cu	1	1.3×10^{-4}	65,000	25.0	Li et al. [26]
	2	2.4×10^{-4}	45,600	28.9	
	3	3.4×10^{-4}	32,000	30.1	
	4	6.2×10^{-4}	22,250	30.9	
	5	9.2×10^{-4}	12,000	31.7	
	6	1.7×10^{-3}	6000	32.5	
	7	3.5×10^{-3}	4700	33.5	
	8	5.3×10^{-3}	10,200	35.4	
	9	7.5×10^{-3}	17,560	37.2	
[233]Ag	1	1.35×10^{-4}	20,000	24.5	Present result
	2	6.7×10^{-4}	10,000	25.4	
	3	1.35×10^{-3}	5000	23.3	
	4	2.7×10^{-3}	4000	27.2	
	5	8.1×10^{-3}	2000	32	
[139]Cu	1	5×10^{-4}	15,000	27.2	Sastry et al. [27]
	2	1×10^{-3}	8000	28.8	
	3	2×10^{-3}	6000	26.9	
	4	7.2×10^{-3}	4000	33	
[128]Ag	1	2.5×10^{-3}		22.5	Sastry et al. [27]
	2	7.5×10^{-3}		28.3	
	3	1.05×10^{-2}		31.4	
	4	1.5×10^{-2}		36.3	
	5	2.0×10^{-2}		39.5	
	6	2.5×10^{-2}		44.8	
[236]Cu	2	2.14×10^{-3}	4000	26.4	Present result

It can be seen from Table 1 that the selected crystals include [233] Ag single crystal and [236], [139] Cu single crystals. In addition, there are also some previous data about [233] Cu single crystal [26] and [128] Ag single crystal [27].

In this work, three comparisons have been made: (1) comparison of the CSS curves between Ag and Cu single crystals with the same orientation [233] or similar orientation [128] and [139] from the present results, as shown in Fig. 4; (2) comparison of the CSS curves between double-slip-oriented single crystal and single-slip-oriented single crystal, whether Cu or Ag; (3) choosing [236] Cu single crystal and [233] Ag single crystal as model materials, comparing their cyclic hardening curves and analyzing their character of surface slip morphologies.

3.1. Cyclic hardening and saturation behavior

Fig. 3 shows the cyclic hardening curves of [233] Ag single crystal and [236] Cu single crystal cyclically deformed at a plastic shear strain amplitude of $\gamma_{pl} = 2.7 \times 10^{-3}$ and $\gamma_{pl} = 2.14 \times 10^{-3}$, respectively. It can be seen from Fig. 3 that for the [236] Cu single crystal, under a similar shear strain amplitude, its resolved shear stress increases slowly with increasing cyclic number and finally develops into a saturation state; however, for the [233] Ag single crystal, its cyclic hardening curve exhibits a clear stress overshooting. The resolved shear stress remains a slow decrease after the stress reaches the first maximum and finally enters into a saturation state. But no matter whether for [236] Cu single crystal or [233] Ag single crystal, the saturation

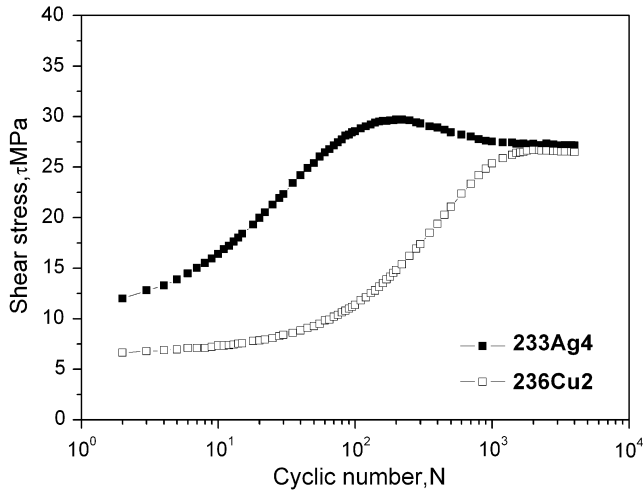


Fig. 3. Cyclic hardening curves of similar oriented Ag and Cu single crystals at the plastic shear strain amplitude of $\gamma_{pl} = 2.7 \times 10^{-3}$ and $\gamma_{pl} = 2.14 \times 10^{-3}$, respectively.

resolved shear stresses are approximately the same. For the two crystals cyclically deformed at other strain amplitudes, similar features can also be seen and are not shown here in detail.

The CSS curves of $[\bar{2}33]$ and $[\bar{1}28]$ Ag single crystals, $[\bar{2}33]$ and $[\bar{1}39]$ Cu single crystals are shown in Fig. 4. It should be especially pointed out that, except for the CSS curve of $[\bar{2}33]$ Cu single crystal, other curves are all fitting ones. In particular, for $[\bar{1}28]$ Ag single crystal, Sastry et al. [27] paid attention only to the CSS curve at the region with high strain amplitude, so in the process of drawing the related CSS curves, the data were borrowed from $[\bar{1}8\bar{1}8]$ and $[\bar{4}59]$ Ag single crystals [28] cyclically deformed at the low strain amplitudes and an extrapolation

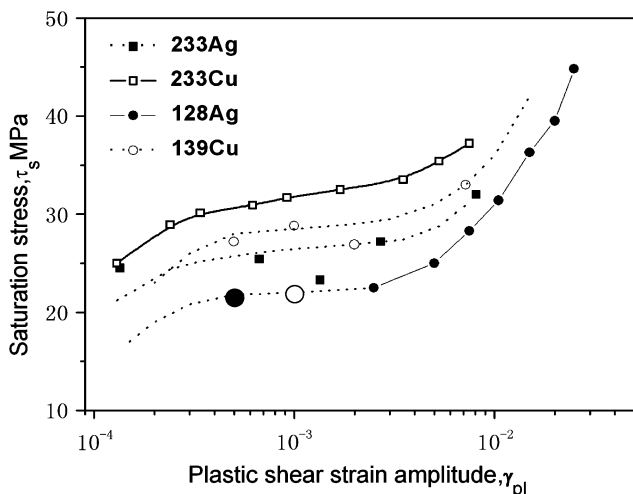


Fig. 4. The CSS curves of Ag and Cu single crystals with similar or same orientations. (Note: the CSS curve of $[\bar{1}28]$ Ag single crystal at low strain amplitudes was made an extrapolation according to our unpublished data of $[\bar{1}8\bar{1}8]$ and $[\bar{4}59]$ Ag single crystals with single-slip orientations at the strain amplitudes of 5.0×10^{-4} and 1.0×10^{-3} , respectively [28].)

tion made of others' data on $[\bar{1}28]$ Ag single crystal in the low strain amplitude range. It is interesting to note that the CSS curve of $[\bar{2}33]$ Ag single crystal shows a slightly increasing plateau region over a plastic shear strain range of 1.35×10^{-4} – 8.1×10^{-3} with an average saturation resolved shear stress of ~ 25 MPa, which is obviously lower than that (~ 31 MPa) of $[\bar{2}33]$ Cu single crystal [26]. Likewise, the average saturation resolved shear stress (~ 22 MPa) of $[\bar{1}28]$ Ag single crystal [27] is still lower than that (28 MPa) of $[\bar{1}39]$ Cu single crystal. It can be concluded that, for the same or similarly oriented single crystal, the saturation resolved shear stress of Cu single crystal is ~ 6 MPa higher than that of Ag single crystal. In addition, for the same kind of crystal, no matter whether for Cu or Ag, it seems that the saturation resolved shear stress of the single crystals with coplanar double-slip orientation is slightly higher (~ 3 MPa) than that of the single crystals with a single-slip orientation, as reported by Li et al. [26]. Meanwhile, the plateau region in the CSS curves of the single-slip-oriented single crystals often seems to be apparent.

3.2. Surface slip morphology

3.2.1. $[\bar{2}33]$ Ag single crystal

Fig. 5 shows the surface slip morphologies of $[\bar{2}33]$ Ag single crystal cyclically deformed at different strain amplitudes. When $\gamma_{pl} = 6.7 \times 10^{-4}$ (see Fig. 5a and b), the primary slip bands (SB) begin to appear in some regions and are distributed inhomogeneously on the specimen surface. Here, the SB are similar to chains and obviously different from the SB in Cu crystals [29–34], which thus can be defined as chain SB. As γ_{pl} increases to 1.35×10^{-3} (see Fig. 5c, d), the SB gradually become dense. In comparison with Ag3 and Ag2 samples, it is apparent that minor intrusions and extrusions appear at lower strain amplitude below $\gamma_{pl} = 6.7 \times 10^{-4}$. Then, these intrusions and extrusions begin to transfer from the irregular point-chain body to regular lamellar structure at a high strain amplitude of $\gamma_{pl} = 1.35 \times 10^{-3}$; the evolution of SB also follows that the SB transfer from chain ones to braid ones. But until this point, a single-slip band is still clearly visible. At a higher strain amplitude of $\gamma_{pl} = 2.7 \times 10^{-3}$ (see Fig. 5e and f), some new braid SB are emerging between certain local bands, which can be defined as developing braid SB. Finally, as γ_{pl} reaches the plateau region above ($\gamma_{pl} = 8.1 \times 10^{-3}$), all the surfaces are covered with the braid SB (see Fig. 5g and h).

3.2.2. $[\bar{2}33]$ Ag and $[\bar{2}36]$ Cu crystals

Fig. 6a, c, e and g shows the surface slip morphologies of $[\bar{2}33]$ Ag single crystal under different magnifications at the plastic strain amplitude of $\gamma_{pl} = 2.7 \times 10^{-3}$. Fig. 6b, d, f and h shows the surface slip morphologies of $[\bar{2}36]$ Cu single crystal under different magnifications at the plastic strain amplitude of $\gamma_{pl} = 2.14 \times 10^{-3}$. By comparing the differences in the surface slip morphologies between Ag

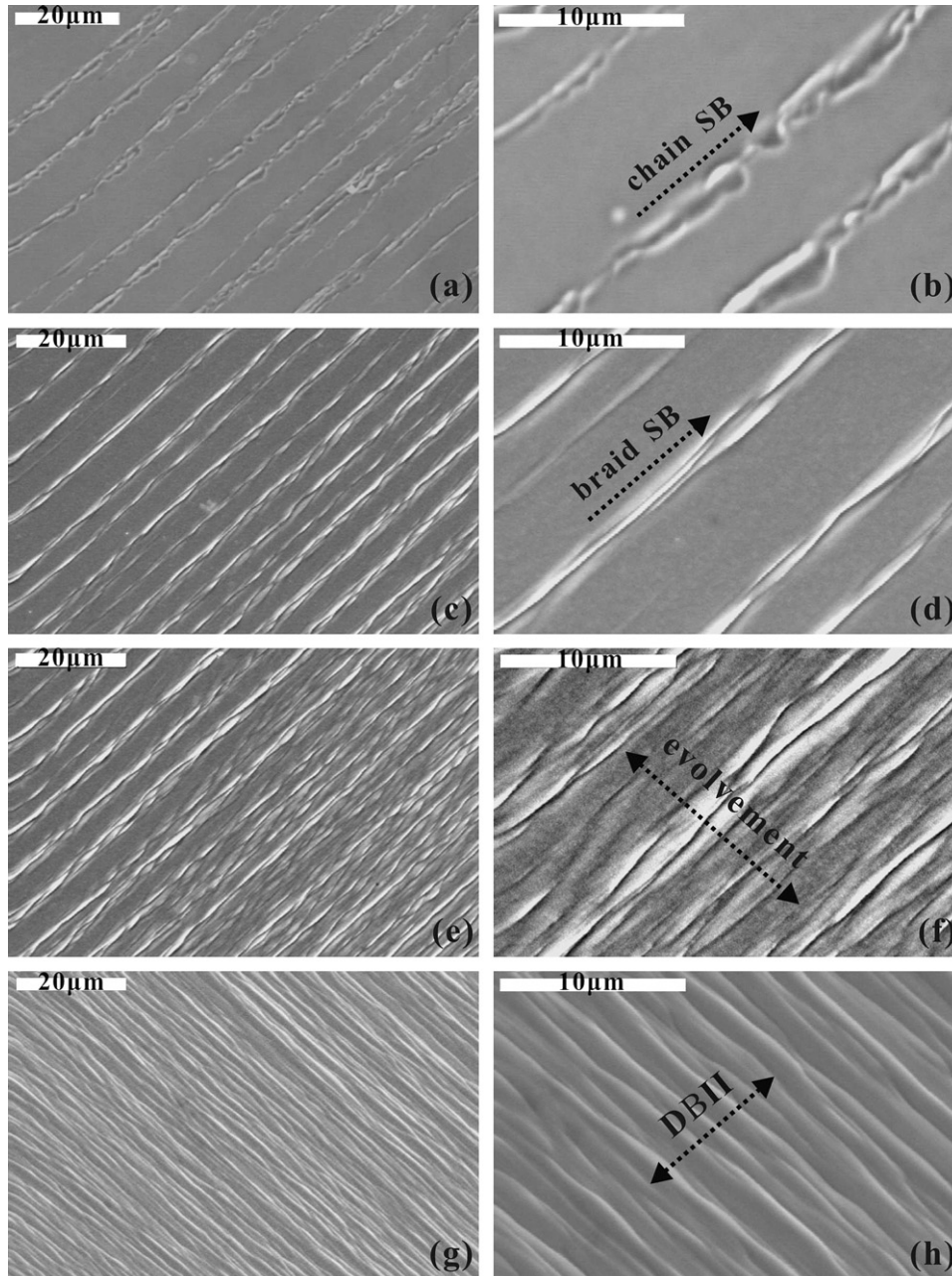


Fig. 5. Surface slip morphologies of the $[233]$ Ag single crystal cyclically deformed at various strain amplitudes: (a) and (b) $\gamma_{pl} = 6.7 \times 10^{-4}$; (c) and (d) $\gamma_{pl} = 1.35 \times 10^{-3}$; (e) and (f) $\gamma_{pl} = 2.7 \times 10^{-3}$; (g) and (h) $\gamma_{pl} = 8.1 \times 10^{-3}$.

and Cu single crystals, one can easily find some interesting features. First, as marked in Fig. 6c and d, α and β represent the interacting angles between DBII and SB in Ag and Cu crystals, respectively. It is apparent that α is $\sim 20\text{--}25^\circ$, and β is close to 90° , indicating $\alpha \ll \beta$. Secondly, as mentioned in Section 3.2.1, the SB in Ag crystals often exhibit seriously intrusive and extrusive states, as the braid SB were observed from the macro-scale morphologies. In contrast, it can be seen that the intrusion and extrusion in Cu crystals are not as obvious as in Ag crystals, therefore, in macro-scale, the SB still show straight lines [29]. Based on the observations above, an interesting question arises: what causes quite different slip morphologies between Cu

and Ag crystals under the same saturation resolved shear stress $\tau_s \approx 26\text{--}27$ MPa?

3.2.3. The interacting angles between DBII and SB

Li et al. [13] pointed out that the habit plane of SB was the (111) plane and the habit plane of DBII was close to the $(\bar{1}01)$ plane, which indicates that DBII and SB should always be perpendicular to each other. However, the analysis in Section 3.2.2 finds that the interacting angles between DBII and SB are not always close to 90° ; sometimes they significantly deviate from the vertical state (see Fig. 6c). Similar phenomena can be also found in the experimental results of other researchers [30–35]. In fact, this is

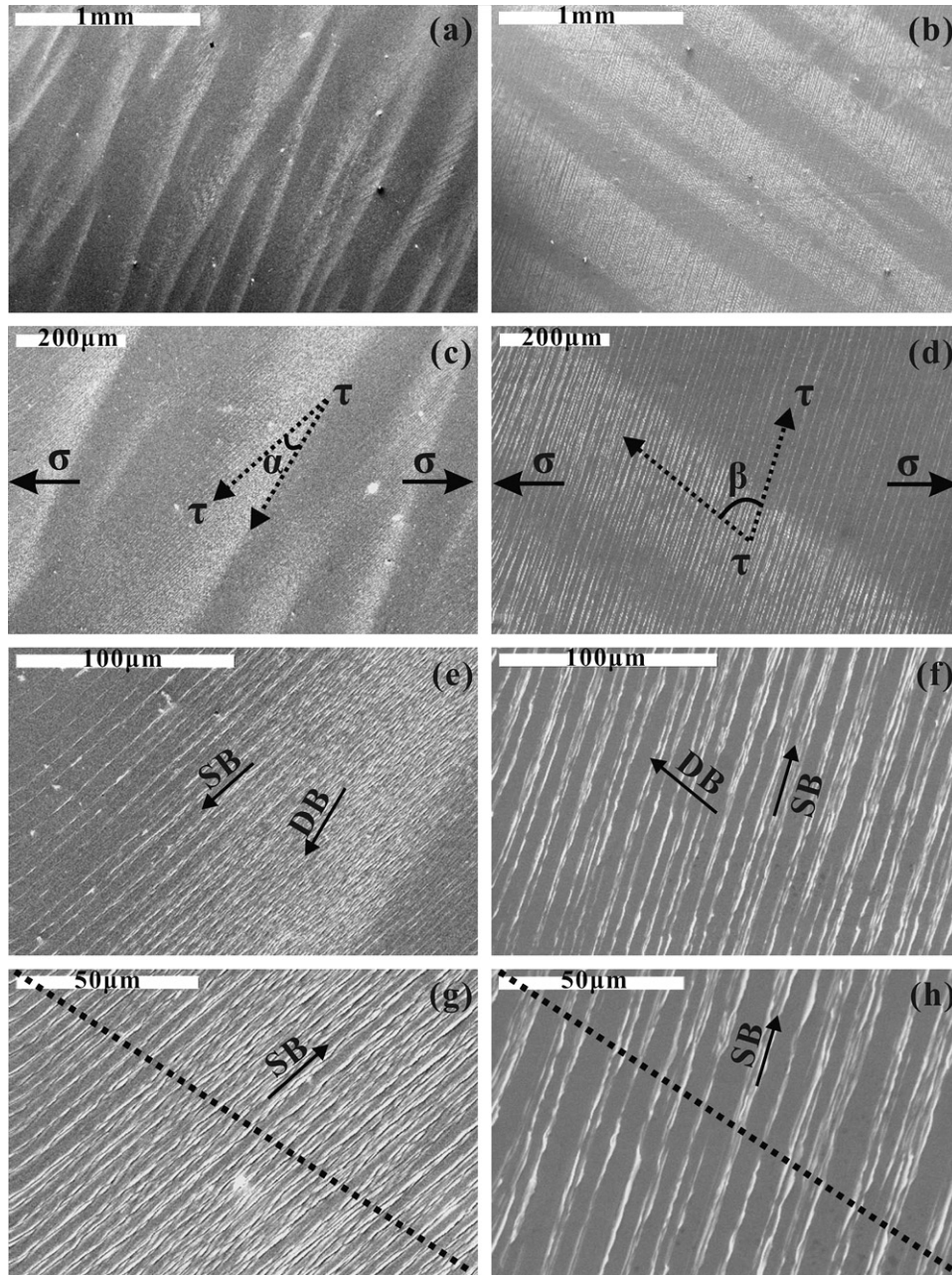


Fig. 6. Surface slip morphologies of $[\bar{2}33]$ Ag single crystal and $[2\bar{3}6]$ Cu single crystal at similar saturation resolved shear stress $\tau_s \approx 26$ MPa. (a), (c), (e) and (g) Ag single crystal cyclically deformed at the plastic strain amplitude of 2.7×10^{-3} ; (b), (d), (f) and (h) Cu single crystal cyclically deformed at the plastic strain amplitude of 2.14×10^{-3} .

due to a difference in the observation planes selected in the special experiment. As shown in Fig. 7a, theoretically the interacting angle between the slip direction and the normal direction of glide plane should be strictly 90° . If one wants to see such a strictly orthogonal angle on the crystal surface, it is absolutely necessary to select an appropriate observation plane, and the normal direction of such an observation plane must be perpendicular to both the slip direction and the normal direction of glide plane. It is well known that the primary slip system of fcc crystals is $(111)[\bar{1}01]$; therefore, after a simple calculation, it can be concluded that the best observation plane is $(\bar{1}\bar{2}1)$ (for a

definition of the best observation plane, refer to Fig. 2 in Murakami [36]). Then the question is: which orientation would more easily intercept the best observation plane $(\bar{1}\bar{2}1)$?

Fig. 7b shows that, if $[1\bar{2}1]$ is regarded as the zone axis, only those orientations coplanar with $[111]$ and $[101]$, such as $[\bar{1}\bar{2}5]$ orientation, will achieve the best observation plane $(\bar{1}\bar{2}1)$ more easily. Such orientations are defined as the best orientations to show the orthogonal relation between DBII and SB. With gradual deviation of the crystal axis away from the best orientation, it becomes impossible for the best observation plane $(\bar{1}\bar{2}1)$ to be intercepted on any

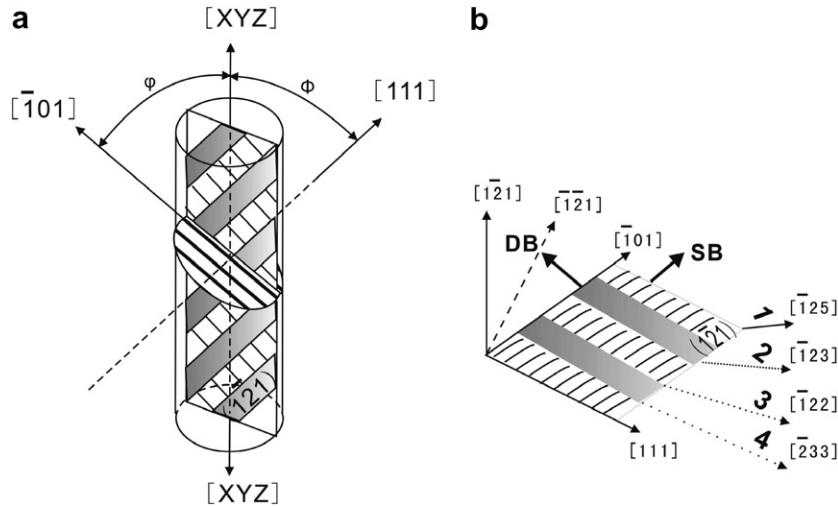


Fig. 7. Relative relationships between crystal orientation, slip direction, normal direction of the glide plane and axial direction of the best suitable observed plane: (a) relative optimal orientation $[XYZ]$; (b) comparison of the four orientations $[\bar{1}25]$, $[\bar{1}23]$, $[\bar{1}22]$ and $[233]$.

lateral surfaces of the specimen. And the interacting angle between DBII and SB on the lateral surface of the specimen will also continue to deviate from 90° (see β , γ , δ in Fig. 8). Jin and Winter [30] and Saletore and Taggart [31] found that the interacting angle between DBII and SB in $[\bar{1}22]$ Cu single crystal was close to 45° . Therefore, it is understandable why the interacting angle between DBII and SB deviates from 90° , and there is no best observation plane, owing to the difference in the crystal orientations.

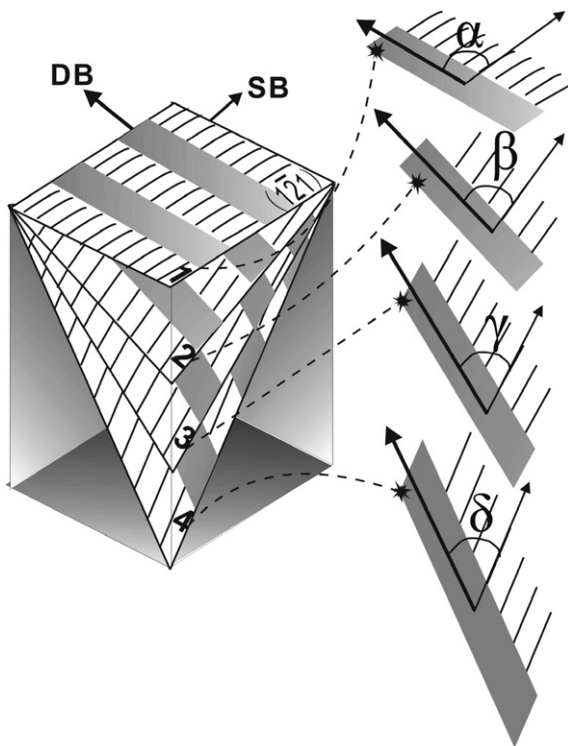


Fig. 8. Illustration of relationship between slip bands and DBII in single crystals with different orientations (α , β , γ and δ correspond to 1, 2, 3, 4 orientation in Fig. 7, respectively).

Finally, the criterion can be summarized by the stereographic triangle (see Fig. 9). As an example for the $(111)[\bar{1}01]$ slip system, the best orientations for observation are located in the shadow of the $[1\bar{2}1]$ zone, which is the arc composed of both $[111]$ and $[\bar{1}01]$ in the stereographic triangle. As the orientation is away from the $[1\bar{2}1]$ zone, it will become more difficult to intercept the $(1\bar{2}1)$ plane, and the interacting angles between DBII and SB will deviate away from 90° . The principle is the same with the other two slip systems, and the criterion map is named as the best observation orientation map. As an example for this study, combining the Schmid factor contours with the best observation orientation map, it is very easy to determine the angle between DBII and SB in differently oriented single crystals. It can be judged from Fig. 9 that $[236]$ is closer to the $[1\bar{2}1]$ zone than $[233]$ is, so the best observation plane intercepted in $[236]$ Cu single crystal is also closer to $(1\bar{2}1)$ than that of $[233]$ Ag single crystal. Therefore, as mentioned above, the interacting angle between DBII and SB in $[236]$ Cu single crystal is closer to 90° ; in contrast, the interacting angle between DBII and SB in $[233]$ Ag single crystal is much less than 90° . The following section investigates whether the difference in the surface slip morphologies of the crystals should be also due to the difference in the crystallographic orientation.

3.2.4. Formation of chain and braid SB

From the orientation relationship between DBII and SB, one can judge that the habit plane of DBII is the $(\bar{1}01)$ plane [13,17] and the possible shear direction is $[111]$, so it can be considered that the applied axial stress σ should be resolved into three stresses, i.e., τ_a , τ_b and τ_c , based on three-dimensional spatial distribution, as illustrated in Fig. 10. It can be seen that τ_a is parallel to the primary slip direction; τ_b is parallel to the shear direction of DBII; and τ_c is perpendicular to the whole

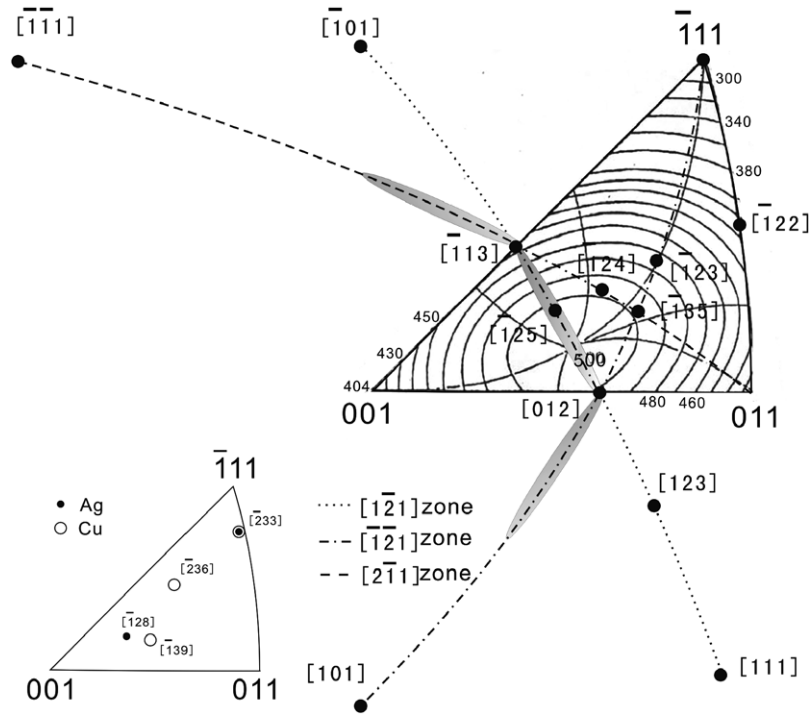


Fig. 9. Criterion map of the angle between slip bands and DBII in differently oriented single crystals. The main map at the upper right-hand corner is formed by the superposition of the Schmid factor contours and the best observation orientation map; the supplementary drawing at the lower left-hand corner is the orientation map of various single crystals involved in this paper.

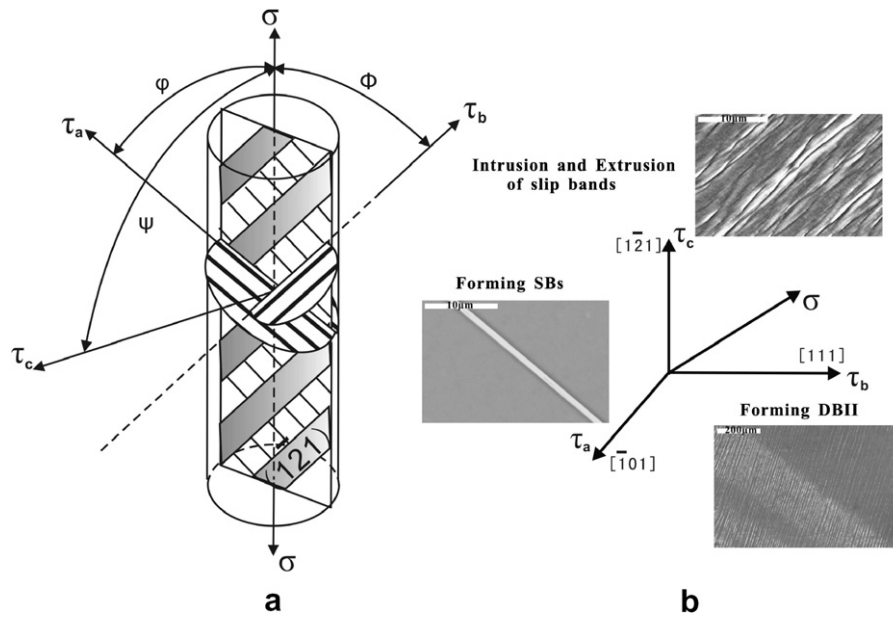


Fig. 10. Illustration of the stresses and slip morphologies in three-dimensional space: (a) the schematic map of the resolution of the axial stress σ into three stresses τ_a , τ_b and τ_c along the slip direction, the normal direction of the glide plane and the normal direction of the best suitable observation plane, respectively; (b) the surface slip morphologies corresponding to each resolved shear stress.

observation plane and represents the normal stress reflecting the extent of the intrusion and extrusion during cyclic deformation. So there is a more clear understanding of how the surface morphology of the fatigued crystal forms, which will allow one to make the following relations:

$$\tau_a = \sigma \cos \phi \cos \phi = \Omega \sigma \tag{1}$$

$$\tau_b = \sigma \cos \phi \cos \phi = \Omega \sigma \tag{2}$$

$$\tau_c = \sigma \cos \psi \cos \phi = E \sigma \tag{3}$$

where ϕ is the interacting angle between the loading direction and the normal direction ($[111]$) of the glide plane; ϕ

is the interacting angle between the loading direction and the slip direction $[\bar{1}01]$; ψ is the interacting angle between the loading direction and the best observation direction $[\bar{1}\bar{2}1]$; $\Omega = \cos \phi \cos \varphi$ is the Schmid factor [37]; and $E = \cos \psi \cos \varphi$ can be defined as extrusion factor. When $\psi = 90^\circ$, $\tau_a = \tau_b = \sigma \cdot \frac{1}{2} \sin 2\phi$ and $\tau_c = 0$; when $\psi = 0^\circ$, $\tau_a = \tau_b = 0$ and $\tau_c = \sigma \cos \phi$.

With variation in the crystallographic orientations away from the best observation orientation $[\bar{1}\bar{2}1]$ zone, the three values of τ_a , τ_b and τ_c will also change. From the comparison between Fig. 11a and b, it is apparent that the axial stress σ along with the orientation variation moves gradually away from the best observation plane $(\bar{1}\bar{2}1)$ consisting of $[111]$ and $[\bar{1}01]$. At the same time, τ_c is gradually increasing, but τ_a and τ_b are relatively reduced. Through the above analysis, it can be concluded that the intrusion and extrusion of the SB on the crystal surface must be more obvious with increasing extrusion factor, $E = \cos \psi \cos \varphi$. And just because of the increasing extent of intrusions and extrusions, clear chain SB and braid SB appear on the crystal surface. This indicates that the loading orientation of the crystal does have a great influence on the surface slip features in the fatigued crystals. With an increasing degree of deviation of the crystallographic orientations

away from the best observation plane, on the one hand, the resolved shear stress τ_c rises, leading to the formation of braid SB on the crystal surface; on the other hand, the deviation of the actual observation plane away from the best observation plane causes the decrease in the intersecting angle between DBII and SB.

3.2.5. The correlation between DBII and SB

The section above discussed the relationship between the crystallographic orientations and the surface deformation morphologies. This section discusses the reason for the formation of DBII and its relationship with the SB. Fig. 12(I) shows the slip morphology of $[\bar{2}33]$ Ag single crystal. When the images a, b and c are intercepted and magnified, the DB, SB and their relation can be clearly seen. In Fig. 12a and c, the SB in DBII have a strong intrusive and extrusive phenomenon, meanwhile the density of SB is also much higher than that in Fig. 12b. This indicates that a higher stress concentration occurs in DBII [5], which is more clearly shown in Cu crystal. Fig. 12(II) shows the surface morphology of $[\bar{2}36]$ Cu single crystal. Being judged from the macro-structural appearance, the bright region in Fig. 12(II) should be DBII. Therefore, this gives rise to the question: what is the difference between the bright and dark regions?

From a series of gradually enlarged images in Fig. 12d, e and f and in comparison with the SB in the dark region, it is well known that the SB in the bright region were broadened and evolved from one to two or more, which can be confirmed by the number of SB across the diagonal. In Fig. 12e and f, the SB at positions 1 and 2 developed from one to two; and the SB at positions 3, 4 and 5 become wider. Thus, it can be presumed that the SB at positions 3, 4 and 5 will evolve from one to two later. In other words, with increasing strain amplitude, each SB will gradually become wider and eventually be divided into two or more. In short, DBII represents an excessive stress concentration; here, a single SB is further widened and ultimately separated into two SB or more, even throughout the entire surface.

4. Conclusions

Based on the experimental results and discussion above, the following conclusions can be drawn:

1. For the same or similarly oriented single crystals, the saturation shear stress of Cu single crystals is ~ 6 MPa higher than that of Ag single crystals. In addition, for the same kind of crystal, no matter whether for Cu or Ag, the saturation resolved shear stress of coplanar double-slip-oriented single crystal is slightly (~ 3 MPa) higher than that of single-slip-oriented single crystal.
2. Schmid factor contours with the best observation map can be used as the criterion to judge the intersecting angle between DBII and SB in the fatigued fcc crystals. As the crystal orientation deviated away

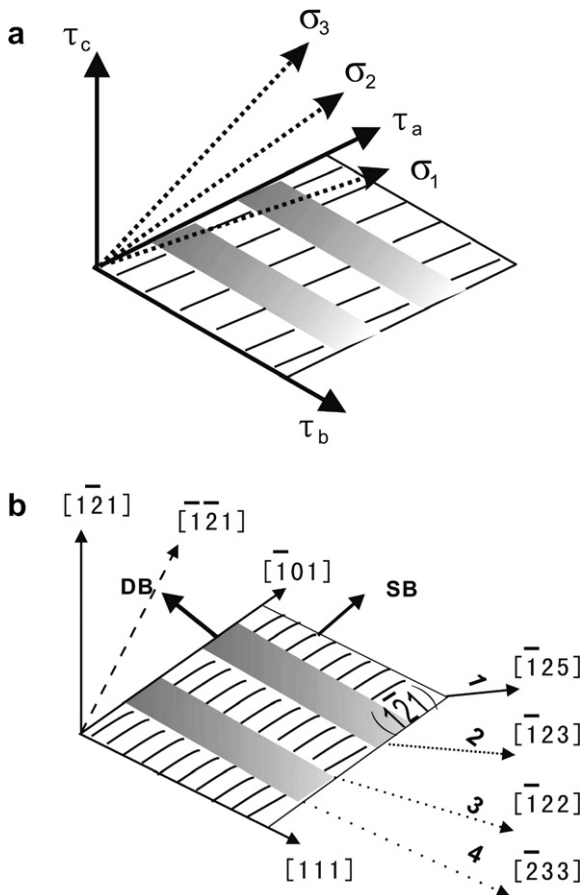


Fig. 11. Evolution map of the resolved shear stresses with the change in orientation: (a) the relationship map between σ and τ ; (b) map of change in orientation.

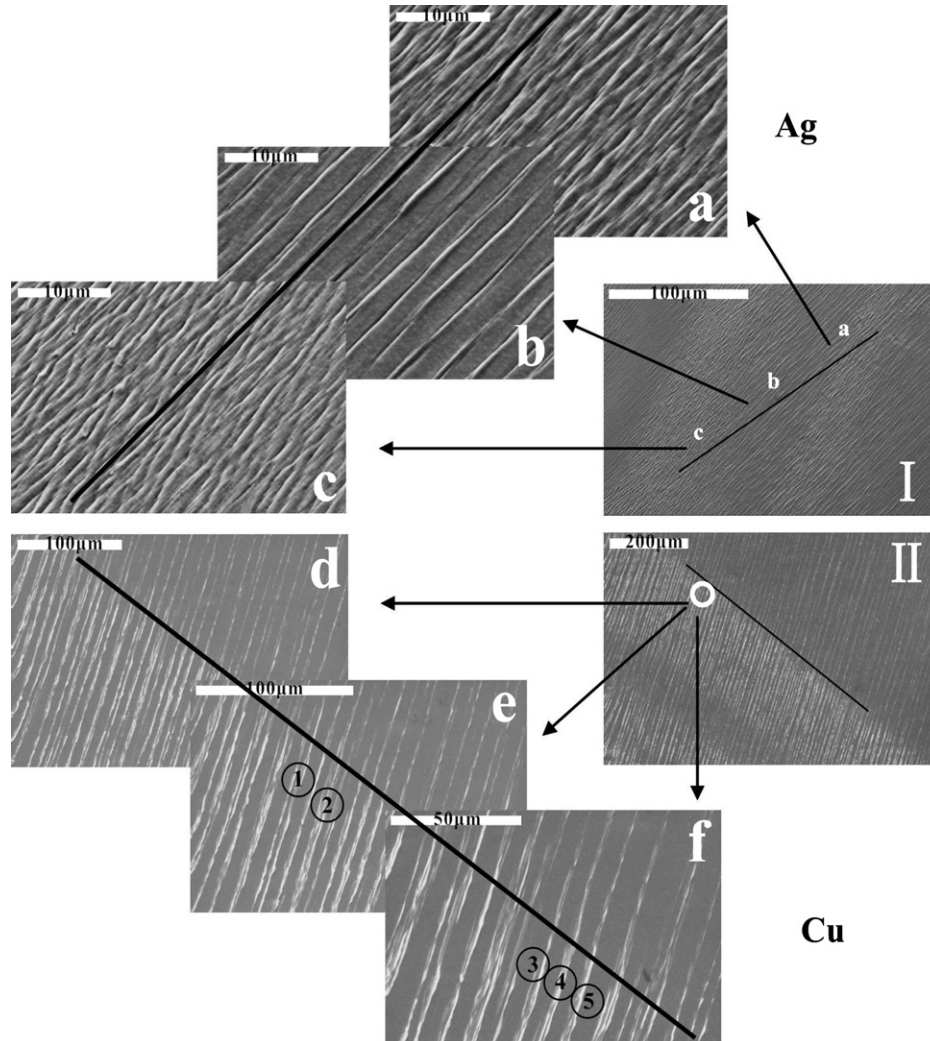


Fig. 12. DBII features of $[\bar{2}33]$ Ag single crystal and $[\bar{2}36]$ Cu single crystal cyclically deformed at different strain amplitudes. (I) (a), (b) and (c) Ag crystal at the plastic strain amplitude of 1.35×10^{-3} ; (II) (d), (e) and (f) Cu crystal at the plastic strain amplitude of 1×10^{-3} .

from the best observation orientation $[1\bar{2}1]$ zone, the interacting angle between DBII and SB will become gradually smaller than 90° ; for example, the interacting angle in $[\bar{2}33]$ Ag single crystals is far less than that in $[\bar{2}36]$ Cu single crystals.

3. With the deviation of the crystallographic orientation away from the observation orientation $[1\bar{2}1]$ zone, the resolved shear stress τ_c along $[1\bar{2}1]$ orientation becomes larger, meanwhile the intrusion and extrusion of the SB also become more obvious, and clear chain SB and braid SB appear on the crystal surface.
4. DBII represents an excessive stress concentration; here, a single slip band is further widened and ultimately separated into two slip bands or more.

Acknowledgements

The authors would like to acknowledge H.H. Su, W. Gao, P. Zhang, H.F. Zou and Q.Q. Duan for the assistance in the experiments. This work was financially supported by

the ‘Hundred of Talents Project’ of the Chinese Academy of Science and the National Outstanding Young Scientist Foundation under Grant No. 50625103.

References

- [1] Basinski SJ, Basinski ZS, Howie A. *Philos Mag* 1969;19:899–924.
- [2] Woods PJ. *Philos Mag* 1973;28:155–91.
- [3] Winter AT. *Philos Mag* 1974;30:719–38.
- [4] Finney JM, Laird C. *Philos Mag* 1975;31:339–66.
- [5] Mughrabi H. *Mater Sci Eng* 1978;33:207–23.
- [6] Abel A. *Mater Sci Eng* 1978;36:117–24.
- [7] Laird C, Finney JM, Kuhlmann WD. *Mater Sci Eng* 1981;50:127–36.
- [8] Cheng AS, Laird C. *Mater Sci Eng* 1981;51:111–21.
- [9] Ackermann F, Kubin LP, Lepinoux J, Mughrabi H. *Acta Metall* 1984;32:715–25.
- [10] Laird C, Charsley P, Mughrabi H. *Mater Sci Eng* 1986;81:433–50.
- [11] Ma BT, Laird C. *Acta Metall* 1989;37:325–36.
- [12] Basinski ZS, Basinski SJ. *Prog Mater Sci* 1992;36:89–148.
- [13] Li SX, Li XW, Zhang ZF, Wang ZG, Lu K. *Philos Mag* 2002;82:3129–47.
- [14] Zhang ZF, Wang ZG, Sun ZM. *Acta Mater* 2001;49:2875–86.

- [15] Neumann P. In: Cahn RW, Hassen P, editors. *Physical metallurgy*. Amsterdam: Elsevier; 1983. p. 1554–93.
- [16] Neumann P. *Mater Sci Eng* 1986;81:465–75.
- [17] Li XW. Effect of crystallographic orientation on cyclic deformation behavior of copper single crystals. Ph.D. thesis, Institute of Metal Research, Chinese Academy of Sciences; 1998.
- [18] Li XW, Wang ZG, Li GY, Wu SD, Li SX. *Acta Mater* 1998;46:4497–505.
- [19] Li XW, Wang ZG, Li SX. *Philos Mag Lett* 1999;79:715–9.
- [20] Li XW, Wang ZG, Li SX. *Philos Mag Lett* 1999;79:869–75.
- [21] Li XW, Zhou Y. *J Mater Sci* 2007;42:4716–9.
- [22] Hostle C. *Philos Mag* 2004;87:299–315.
- [23] Vorren O, Ryum N. *Acta Metall* 1987;35:855–66.
- [24] Wu XM, Wang ZG, Li GY. *Mater Sci Eng* 2001;314:39–47.
- [25] Mughrabi H, Ackermann F, Herz K. In: Fong JT, editor. *Fatigue mechanisms*. ASTM STP 675. Philadelphia: ASTM; 1979. p. 69–105.
- [26] Li XW, Wang ZG, Li SX. *Mater Sci Eng* 1999;260:132–8.
- [27] Sastry SML, Ramaswami B, Goetz F. *Metall Trans* 1976;7:243–8.
- [28] Li P, Zhang ZF, Li SX, Wang ZG [submitted for publication].
- [29] Jia WP, Li SX, Wang ZG, Li XW, Li GY. *Acta Mater* 1999;47:2165–76.
- [30] Jin NY, Winter AT. *Acta Metall* 1984;32:989–95.
- [31] Saletore M, Taggart R. *Mater Sci Eng* 1978;36:259–70.
- [32] Zhang ZF, Wang ZG. *Acta Mater* 1998;46:5063–72.
- [33] Zhang ZF, Wang ZG, Hu YM. *Mater Sci Eng* 1999;272:410–7.
- [34] Li XW, Wang ZG, Li SX. *Mater Sci Eng* 1999;265:18–24.
- [35] Buque C. *Int J Fatigue* 2001;23:671–8.
- [36] Murakami Y, Mura T, Kobayashi M. In: Fong JT, Fields RJ, editors. *Basic questions in fatigue*. STM STP 924, vol. 1. Philadelphia: ASTM; 1988. p. 39–63.
- [37] Suresh S. *Fatigue of materials*. 2nd ed. Cambridge: Cambridge University Press; 1998. p. 22.